

# Polars Changing State: Multiwavelength Long Term Photometry and Spectroscopy of QS Tel, V834 Cen, and BL Hyi

Jill R. Gerke<sup>1</sup>

Steve B. Howell<sup>2</sup>

Frederick M. Walter<sup>3</sup>

Received \_\_\_\_\_; accepted \_\_\_\_\_

---

<sup>1</sup>Department of Astronomy, University of Arizona, Steward Observatory, 933 N. Cherry Ave., Tucson, AZ 85721; jgerke@email.arizona.edu

<sup>2</sup>WIYN Observatory & NOAO, P.O. Box 26732, 950 N. Cherry Ave., Tucson, AZ 85726-6732; howell@noao.edu

<sup>3</sup>Department of Physics and Astronomy, Stony Brook University, Stony Brook, NY 11794-3800

## ABSTRACT

Long term optical and near-infrared photometric and blue spectroscopic observations were obtained for QS Tel, V834 Cen, and BL Hyi. The optical light curves of all three polars displayed large magnitude changes during our observations. These same high/low state transitions were also apparent in near-infrared *JHK* photometry, though with decreased amplitude. The color of the polar with respect to its state was examined and found not to be a good indicator of the instantaneous state. During low to high state transitions, a nearly constant magnitude difference was observed in all three polars. This  $\Delta m$  value was found to be consistent with the level expected to occur if accretion onto the white dwarf reached the Eddington luminosity during the high state. The high state Balmer decrement was measured for each star and used to estimate that the temperature of the emission line forming region was  $\sim 12,000\text{K}$  with  $N_H$  near 12.8 dex. No relationship between the Balmer emission line strength and the white dwarf magnetic field strength was seen, in contrast to a good correlation between these two parameters observed for UV emission lines.

*Subject headings:* binaries: general - novae, cataclysmic variables - stars: individual(QS Telescopii, BL Hydri, V834 Centauri) - stars:magnetic fields

## 1. Introduction

Polars, or AM Her stars, are a subclass of cataclysmic variable consisting of a close, interacting binary system containing a white dwarf primary having a magnetic field on the order of 10-200 MG (Ramsay et al. 2004). The white dwarf is paired with a low-mass main sequence secondary and both stars are tidally locked with the binary period which is generally between 80 minutes and 4 hours (Warner 1995). The secondary acts as a mass donor for the white dwarf, overflowing its Roche lobe and transferring mass at the inner Lagrangian point.

The transferred mass, unable to form an accretion disk due to the white dwarf's high magnetic field (Araujo-Betancor et al. 2005), instead forms an accretion column. The infalling matter, funneled by the magnetic field, forms a shock region above the magnetic pole. The material then continues, at a lower velocity, to the white dwarf surface where it accretes over a small area covering only a few thousand square kilometers near the magnetic pole (Howell et al. 1999). The shock region and the post shock flow to the white dwarf surface comprise the accretion column (Cropper 1990).

Due to the lack of an accretion disk around the white dwarf, the rate of accretion onto the primary is equal to the instantaneous rate of mass loss ( $\dot{M}$ ) by the secondary star (King & Cannizzo 1998). Consequentially, polars vary in luminosity in direct relation to  $\dot{M}$ . This is different from other cataclysmic variables that have accretion disks, wherein the effects of a changing rate of mass transfer from the secondary star are more subtle.

The high/low state luminosity variation of a polar results from differing rates of accretion onto the primary and can be traced back to differing rates of mass transfer from the secondary. We note that polars can also show intermediate states (Howell et al. 2002). The duration of a state can be a matter of weeks, months or years. Although it is uncertain whether conditions on the secondary actually cause the low state, star spots or stellar

activity in general, could be responsible for the decrease in accretion (Araujo-Betancor et al. 2005). During a high state, the mass transfer rate in polars is typically near  $10^{-10}M_{\odot}\text{yr}^{-1}$  (Howell et al. 1999). During a low state, even though mass transfer due to Roche lobe overflow may end completely (Howell et al. 1999), accretion via winds from the secondary is possible (Kafka et al. 2005).

During the high state, the emission from the X-ray through the optical and IR bands is dominated by accretion flux. The difference in optical magnitude between a high state and low state of a polar is typically near 2-2.5 magnitudes. For example, Kafka et al. (2005) showed that AM Her changed approximately 2 mag between states and out of fourteen polars surveyed by Ramsay et al. (2004), twelve had a change in magnitude within the 1.5-3.0 mag range; the average change was  $2.1 \pm .2$  mag. Despite any differences in the white dwarf’s magnetic field strength or other parameters governing the polar, the comparable change in luminosity at the change of state suggests there is some similarity in the cause and behavior of the high state luminosity emitted at or near the accretion region of polars.

In order to understand this similarity in luminosity change and the behavior of the change of state of polars we undertook a long term study involving observations from the SMARTS<sup>1</sup> facilities. Our observations consisted of optical (B, V and I) and infrared (J, H and K) light curves along with blue (3500-5300Å) spectra of several polars.

In the following sections, examination of the optical light curves and blue spectroscopic data obtained from the study for QS Tel, BL Hyi and V834 Cen leads us to propose a model where the accretion region on the white dwarf reaches the Eddington luminosity in

---

<sup>1</sup>SMARTS, the Small and Medium Aperture Research Telescope Facility, is a consortium of universities and research institutions that operate the small telescopes at Cerro Tololo under contract with AURA.

the high state. We note that system color is not dominated by high/low state conditions, in the optical or the near-IR. From the spectroscopic data, the Balmer decrement ( $H\gamma/H\beta$ ) is determined for the high state of a polar and used to find the high state temperature and density of the emitting material. We also examine the emission line strengths with respect to the strength of the white dwarf magnetic field.

## 2. Observations and Data Reduction

All the data we report herein were obtained with the SMARTS facilities at Cerro Tololo by the SMARTS service observers. All dates below refer to the civil date at the start of the night. In addition to QS Tel, BL Hyi and V834 Cen, we also monitored EF Eri and VV Pup. These two polars, however, remained in the low state for the duration of this study and therefore are not discussed further here.

### 2.1. Imaging

We obtained images of the targets using the ANDICAM<sup>2</sup> dual-channel photometer on the 1.3m telescope. The optical detector is a 1024x1024 CCD; the near-IR channel uses a Rockwell 1024x1024 HgCdTe Hawaii array. The optical and near-IR channels operate independently, so we can take a set of near-IR images while integrating in the optical.

We obtained data on many nights between 2003 August and 2005 January (see Table 1). The optical data consisted of single images through B, V, and I filters. Integration times were 100 seconds per filter (200 seconds for QS Tel). The near-IR images consisted of three dithered 27 second integrations through each of the J, H, and K (CIT/CTIO) filters.

---

<sup>2</sup><http://www.astronomy.ohio-state.edu/ANDICAM/detectors.html>

Images are obtained sequentially through each of the filters, with the  $B$  and  $J$ ,  $V$  and  $H$ , and  $I$  and  $K$  pairs obtained simultaneously. QS Tel was too faint to obtain reliable  $JHK$  photometry.

The optical ANDICAM data are processed (overscan subtraction and flat-fielding) prior to distribution. Because we obtained only single images through each filter each night, the noise is dominated, in some cases, by cosmic rays and hot pixels. Aside from a 2x2 rebinning, the IR data are delivered raw. We generate the flat field images from the dome flats obtained about every other night. We generate a sky image by taking the median of the dithered images. We subtract the sky image from the individual frames, then shift and add the individual frames.

Standard practice is to use ANDICAM for differential photometry, but the SMARTS project routinely obtains images of optical and near-IR standard fields on photometric nights to allow defined zero-points for the photometry. Our optical light curves consist of relative magnitudes and the color measurements are instrumental. The near-infrared values, however, are calibrated magnitudes, so we quote true color values.

## 2.2. Spectroscopy

The spectra (Table 1) were obtained with the RC spectrograph on the 1.5m telescope. This is a slit spectrograph, with a 300'' long slit oriented E-W. The stars are always observed through a 110 $\mu$ m (1.5'') slit and obtained three images at each epoch in order to filter cosmic rays. Each set of images is accompanied by a wavelength calibration arc lamp exposure. We have developed a pipeline, written in IDL, to process the data. The pipeline subtracts the overscan, and divides by the normalized flat field image.

A median image is generated from the three images and we extract the spectra,

both by using an unweighted boxcar extraction and by fitting a Gaussian profile at each wavelength. For the boxcar extraction, we determine the width of the extraction box by fitting a Gaussian to the spatial profile, and the background is measured to either side of the source. In the Gaussian extraction we fit a Gaussian to the spatial profile at each wavelength, and retain the number of counts in the fit. This is less sensitive to noise in individual pixels, and provides a higher S/N spectrum.

A spectrophotometric standard, either LTT 4364 (Hamuy et al. 1992, 1994) or Feige 110 (Oke 1990; Hamuy et al. 1992, 1994), was observed each night in order to convert the counts spectrum to a flux spectrum. We note that there will be systematic deviations at the blue end of the spectrum when the targets and standard are observed at different air masses, because the slit orientation is fixed and not free to rotate with the parallactic angle. This effect is largest for BL Hyi, but has no significant effect on any of our conclusions. Due to seeing-related slit losses, we do not obtain absolute fluxes, but rather use the standard star to recover the shape of the continuum and provide relative fluxes.

Most of the spectra were obtained with grating 26 in first order, which provides  $4.3\text{\AA}$  resolution between 3600 and  $5200\text{\AA}$ . Some spectra were taken in first order using grating 47 and the GG 495 order sorting filter to obtain  $3.1\text{\AA}$  resolution between 5650 and  $6970\text{\AA}$ . This resolution is sufficient to resolve the  $H\alpha$  line.

### 3. Photometric Analysis

Figure 1 shows the optical light curves for QS Tel, BL Hyi and V834 Cen, with both the state of the system and the boundaries used to define those states indicated. The luminosity boundaries seen in Figure 1 for the states of the polars were not difficult to determine, as each polar had a baseline low state luminosity with only small variations due to the

heterogeneous nature of the accretion stream or flares from the secondary (see Ramsay et al. 2004; Howell et al. 2002; Kafka et al. 2005 for further explanation). To compensate for flares and for observations taken when the polar was changing states, we placed some of the photometric measurements in a “transitional region” between the well defined high and low states for QS Tel and V834 Cen (see Figure 1). The change of state for BL Hyi occurs between observations and does not show transitional points. However, the high state does contain a variation of about 0.2 magnitudes caused by an orbital modulation as the active pole rotates in and out of view (Wolff 1999).

Figure 2 and Figure 3 show the J, H and K band light curves for BL Hyi and V834 Cen, respectively. The near-infrared light curves show brightness changes coincident with, though of lesser amplitude than, the high/low optical light curve changes. This correlation indicates that accretion flux can be a major factor in the near-infrared brightness of a polar, despite the presence of a red secondary. Orbital modulation is visible in the near-IR high state light curves of BL Hyi just as it was in the optical.

As Figure 1 shows the change in B magnitude between the low state and the high state for each polar is  $\sim 2$ -2.5 magnitudes. As stated above, this level of brightness change is similar to that observed for many other polars as well. In order to determine a possible explanation for the consistency of the change in luminosity between high and low states in polars, the Eddington luminosity was considered as a possible limiting factor for the luminosity of the accretion process (see §3.2).

### 3.1. Color of the Polars

The SMARTS photometric observations were used to create color-color plots where the state of the polar at the time of the observation is indicated (Figures 4 & 5). We noted



the state of each observation in order to determine whether color could be used as a good indicator of the accretion state. While there is some connection between color and state, the results are not consistent for all polars.

The optical data of QS Tel is grouped according to state in the color-color plot. The SMARTS observations show QS Tel becoming progressively bluer as it moves from the low to the transitional and into the high state. These color groupings confirm the accretion region dominates the optical light in the high state causing the system to appear more blue. In the low state, some spectral combination of the white dwarf and the secondary star occurs resulting in a redder color. During this time, the red secondary contributes a higher fraction of the optical light while the cooling accretion region contributes less. The relatively small range in color for QS Tel may be the result of the hot white dwarf ( $T_{eff}=17500\text{K}$ , Rosen et al. 2001) dominating the optical in the low state as well as the high state.

The spread of the data according to high and low state for V834 and BL Hyi (Figures 4 & 5) suggest a more complex spectral relationship between the white dwarf and the secondary as the system goes from a high state to a low state. In the optical, the transitional state of V834 Cen is redder than either the low or high state. While the high state appears to be slightly bluer than the low state, there is some overlap. The overlap of the range of colors for the high and low states could be a result of the secondary and the white dwarf both contributing to create a complex spectral energy distribution in the low state. In the near-IR, however, there is less overlap in the color between states and the color of the transitional state separates the bluer color of the high and redder color of the low state.

The results from BL Hyi also appear to be complex. The high state has a range of colors from red to blue while the low state observations all show a similar color that is bluer than the color of the high state in  $(V-I)_i$ , but redder in  $(B-V)_i$ . The high state data of BL

Hyi has a larger spread toward the red than is seen with the other systems, likely caused by color modulation over the orbital period due to self eclipse of the accretion region, where the amplitude has been shown to increase with increasing wavelength (Warner 1995). This argument is supported by the near-IR color plot which also shows the high state covering a range from red to blue.

In the above discussion of high and low state color, we have not yet added effects due to cyclotron humps. During low states, these wide ( $\sim 1000\text{\AA}$ ) continuum humps can provide strong effects at specific wavelengths. The location and strength of cyclotron humps vary from system to system as well as over orbital phase. The amplitude of the humps depends mainly on the mass transfer rate, with the largest amplitudes generally occurring during the low state. Given the range of the observed colors in the high and low states, we conclude that the color of a polar can not be used alone as a good indicator of its accretion state.

### 3.2. Eddington Luminosity

The Eddington luminosity for accretion onto the white dwarf in each of our observed polars has been calculated using stellar parameters taken from the literature (see Table 2). The Eddington Luminosity ( $L_E$ ) is given by

$$L_E = \frac{4\pi GcM_{WD}}{k}$$

where  $G$  is the gravitational constant,  $M_{WD}$  is the mass of the white dwarf and  $c$  is the speed of light. The opacity of the accreting matter ( $k$ ) was estimated to be  $1.2 \text{ cm}^2\text{g}^{-1}$ , assuming a hydrogen mass fraction of 1 (Warner 1995).

The change in state of a polar is due to changes in the mass transfer rate, however material only accretes over a small region near the magnetic pole, the accretion region. Thus, only that fractional area of the white dwarf, estimated to be  $\sim 10\%$  of the surface area

of the white dwarf, changes luminosity appreciably. Due to the similarity in white dwarf mass and composition, the Eddington luminosities will also be similar. This similarity results in a change in magnitude at the change of state that is approximately uniform for many polars.

While the accretion region reaches its peak luminosity in the high state due to the heightened rate of mass transfer, the luminosity of the rest of the white dwarf remains essentially unchanged from that of the low state. The resulting high state luminosity ( $L_H$ ) of the polar can be estimated as  $L_H = .9L_P + .1L_{PE} + L_S$  where  $L_P$  is the low state luminosity of the primary,  $L_{PE}$  is the estimated Eddington luminosity of the primary, and  $L_S$  is the luminosity of the secondary. The coefficients refer to the percentage of the surface area of the star with that luminosity. In the low state, the accretion region receives a negligible amount of matter, therefore the accretion region is not heated measurably and the entire surface area of the primary has approximately the same luminosity  $L_L = L_P + L_S$  where  $L_L$  is the low state luminosity. To summarize, our toy model proposes that during the low state the entire white dwarf has nearly the same luminosity (i.e., a uniform surface temperature), while during the high state the luminosity of the accretion region increases to the Eddington luminosity and the luminosity of the rest of the star remains unchanged.

Using the above expressions for the high state and low state luminosities of a polar, the change in luminosity due to a change to a high state is determined. The low state luminosity of the primary is estimated by the low state luminosity of the system,  $L_L = L_P$  (assuming an optically dim secondary) and the change in luminosity is estimated as  $.1L_{PE} - .1L_L$ . The Eddington luminosity was then converted to an apparent magnitude using the polar distances from Table 2 and the predicted change in magnitude was calculated with the results shown in the final column of Table 2.

The light curves of BL Hyi, QS Tel and V834 Cen (Figure 1) show a change of about 2

magnitudes, however, our simple model predicts a slightly smaller change in luminosity for these polars. The Eddington luminosity gives the maximum radiative luminosity that can be supported by an object with a stable, isotropic, homogeneous and fully ionized atmosphere (Moon et al. 2003). These atmospheric conditions do not strictly apply to the white dwarf of a polar since the accretion column is inhomogeneous and covers a small portion of the white dwarf. In addition, the accretion region does not cool off instantaneously to the white dwarf temperature. We have also ignored other details such as possible emission through the sides of the column or from the accretion stream.

The realistic, complex details of the atmosphere above the accretion region may make our calculations an underestimate of the change in magnitude due to the change to a high state. Also, the size of the accretion region could be overestimated (Warner 1995), which would in turn cause the change in magnitude to be overestimated, plus some polars may have more than one active accretion region at one time. Finally, by assuming an optically dim secondary, the change in magnitude is underestimated by one tenth the optical magnitude of the secondary star ( $0.1L_S$ ).

#### 4. Spectroscopic Analysis

A representative SMARTS spectrum from the high state and the low state of BL Hyi can be seen in Figures 6 & 7, respectively. The high state and low state are easily distinguishable as the high state has discernible, strong emission lines, while the low state does not.

#### 4.1. $H\gamma/H\beta$ Decrement

By calculating the Balmer decrement ( $H\gamma/H\beta$ ) for the high state spectra, ranges for the temperature and density within the emission line forming region can be estimated. Williams (1991) modeled the Balmer decrement for emission lines in cataclysmic variables using grids of specific temperature, density, and inclination. While Williams’s work was for line forming regions in accretion disk chromospheres, the same temperature-density relations should hold for the line forming regions in the accretion stream, a chromosphere-like area above and near an accretion pole. William’s Balmer decrements, averaged over inclination, are shown in Figure 8. Figure 9 plots the high state decrements determined from our SMARTS polar spectra over a time interval of about 500 days.

Using the optical data (Fig. 1) to define the state, we calculated the average Balmer decrement for the high state of each polar. Table 3 gives our results for the  $H\gamma/H\beta$  decrement for each star, along with the estimated temperatures and number density of hydrogen drawn from Williams (1991). The high state emission line forming regions of the polars are found to be similarly hot (10,000-15,000K) and dense (12.4-13.2 dex). This is in good agreement with Warner (1995).

#### 4.2. Emission Line and Magnetic Field Strength

Using high state spectroscopic observations of polars obtained by the *International Ultraviolet Explorer* (IUE), Howell et al. (1999) compared the strength of several UV emission lines to the magnetic field strength of the white dwarf for a number of polars. They found that the UV emission line strength decreased with increasing magnetic field strength. The same process used by Howell et al. (1999) for UV emission lines was applied to our current spectroscopic dataset.

Using spectra obtained on nights listed as clear (to avoid decreased emission line strength due to clouds) an average high state emission line flux was determined for  $H\beta$ ,  $H\gamma$ , and  $H\delta$  for each of our three polars. The average emission line fluxes were then converted into average line luminosities, using the distances given in Table 2, with our results compiled in Table 4. Comparing line strength to the magnetic field strength of each polar, we find that the trend of decreasing line strength with increasing magnetic field seen in the UV is not evident in the Balmer lines.

Within the uncertainties, all three polars show similar strength Balmer emission lines. This inconsistency with the results of Howell et al. (1999) likely indicates that the strength of the optical emission lines are less directly affected by the magnetic field strength compared with those in the UV. The Balmer emission is likely to be more effected by the local conditions under which they form in the accretion stream and column. The location of the emission line forming regions must also be considered. The UV lines form lower in the accretion column, nearer to the magnetic pole. The optical emission lines, on the other hand, form in a region in the accretion stream with a weaker magnetic field and an environment of varying temperature and density.

## 5. Conclusion

The lack of an accretion disk around the white dwarf in a polar directly relates the rate of mass transfer from the secondary to the rate of mass accretion onto the primary. Therefore, when mass transfer from the secondary slows, accretion onto the primary also slows and the luminosity of the polar changes. A change of state is generally characterized by a change in the optical brightness of  $\sim 2$ - $2.5$  magnitudes. The consistency in magnitude change at the change of state for most polars is consistent with the accretion region reaching the Eddington luminosity in the high state.

The color-color relations in both the optical and near-IR show different color trends for each polar over the different states. The optical color of QS Tel shows a polar which is blue in the high state, redder in the low state, with the transitional region falling between the two. Colors in both the optical and near-IR for V834 Cen and BL Hyi show a complex relationship between high and low states. The near-IR light curves also show a change in luminosity at the change of state, however the luminosity change is smaller than in the optical and decreases when moving from the J to the K bands.

The Balmer decrement ( $H\gamma/H\beta$ ) determined from high state spectroscopy, reveals that the emission line forming regions are hot (8000-15000K) and fairly dense ( $\text{Log } N_H=12.4-13.2$ ). We also measured the Balmer line emission strength, finding no clear relationship to the magnetic field strength of the polar. In order to compare the states of a polar and to determine how parameters change during a state change, long term studies are needed. These systems are dynamic and must be monitored to increase understanding of their properties.

We wish to thank the SMART consortium for their kind allocation of telescope time and the SMART observers for their diligence and hard work in obtaining the data used herein. We would also like to thank the anonymous referee for their helpful comments and suggestions.

Table 1. Observation Log

Star	ANDICAM		Spectrograph	
	Nights	Span (UT)	Nights	Span (UT)
QS Tel	73	2003 Aug 21 - 2004 Oct 28	38	2003 Aug 14 - 2005 Jun 03
Bl Hyi	74	2003 Aug 21 - 2005 Jan 26	76	2003 Aug 19 - 2005 Jun 03
V834 Cen	48	2004 Jan 13 - 2004 Sep 18	44	2004 Jan 20 - 2005 Jun 05

Table 2. Eddington Luminosity Parameters

Star	Mass of White Dwarf	Distance (pc)	Low State $V$ Magnitude	Eddington Luminosity (ergs/s)	$\Delta$ Magnitude
QS Tel	$0.71 M_{\odot}^1$	$170^1$	$17.3^4$	6E37	1.7
Bl Hyi	$0.50 M_{\odot}^2$	$132^2$	$17.4^5$	4E37	1.7
V834 Cen	$0.64 M_{\odot}^3$	$80^3$	$16.9^5$	5E37	1.8

References. — (1) Rosen et al. 2001; (2) Wolff et al. 1999; (3) Mauche 2002; (4) Ferrario et al. 1994; (5) Araujo-Betancor et al. 2005.



Table 3. High State Temperature and Density Ranges based on the Balmer Decrement  
( $H\gamma/H\beta$ )

Star	$H\gamma/H\beta$	Temperature (K)	Log $N_H$
QS Tel	$.83\pm.04$	10000	13.0
		15000	12.8
BL Hyi	$.80\pm.002$	10000	12.5
		15000	12.4
V834 Cen	$1.01\pm.02$	10000	13.2
		15000	13.0

Table 4. Magnetic Field Strength and Optical Emission Line Luminosity

Star	Magnetic field (MG)	Log Average Line Luminosity		
		$H\beta$	$H\gamma$	$H\delta$
QS Tel	$56^1$	$29.24\pm.09$	$29.29\pm.12$	$29.18\pm.08$
BL Hyi	$23^2$	$29.44\pm.08$	$29.12\pm.19$	$29.07\pm.10$
V834 Cen	$31^3$	$29.32\pm.16$	$29.30\pm.15$	$29.32\pm.17$

References. — (1) Ferrario et al. 1994; (2) Ferrario et al. 1996; (3) Ferrario et al. 1992.

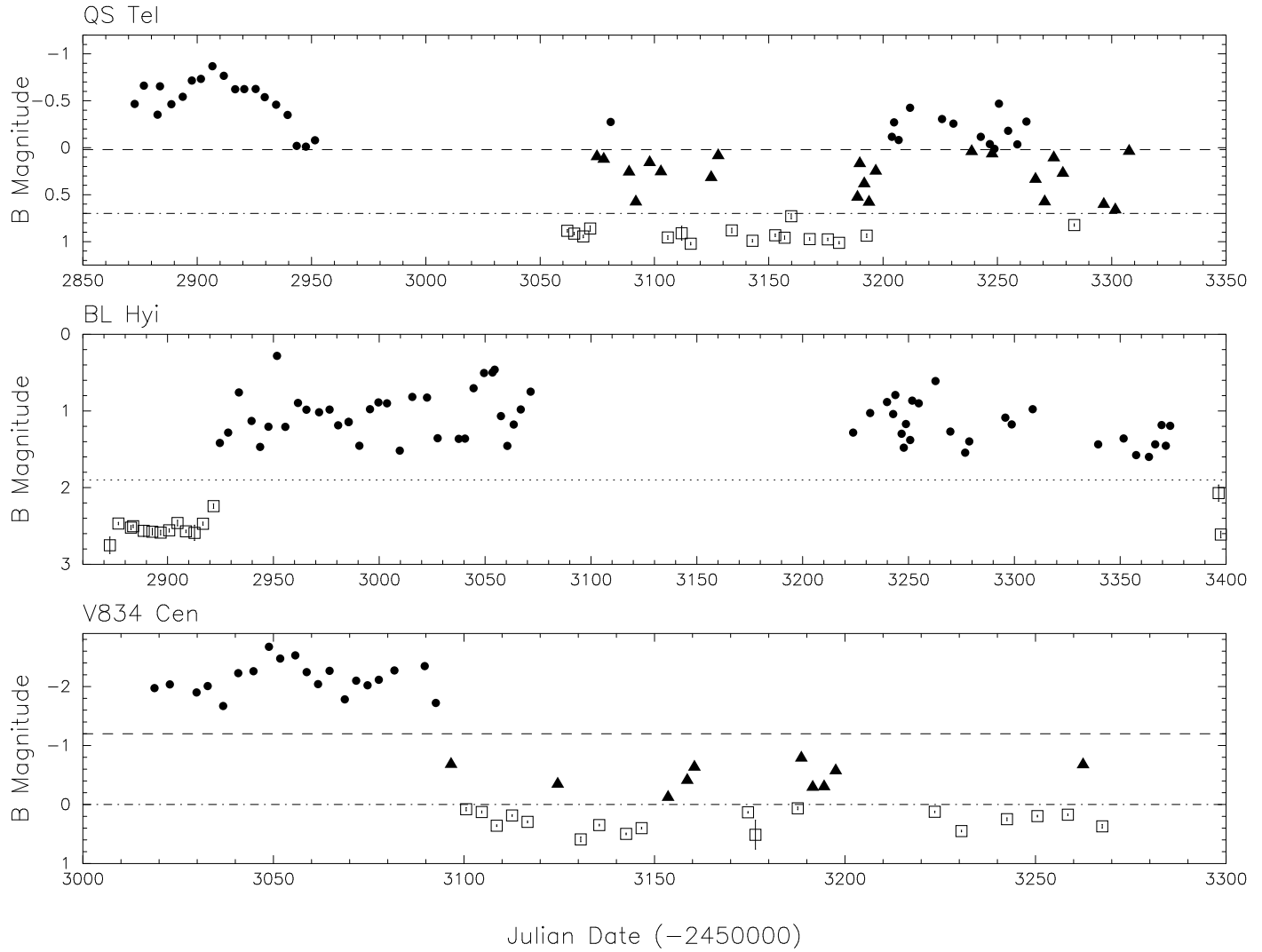


Fig. 1.— Light curves in relative B Magnitude vs Julian Date.  $\blacktriangle$  Transition;  $\square$  Low state;  $\bullet$  High state. The dashed line indicates the lower limit to the high states while the dot-dashed line indicated the upper limit to the low state. Points between the lines are the transition region. BL Hyi shows a clean low to high state transition.

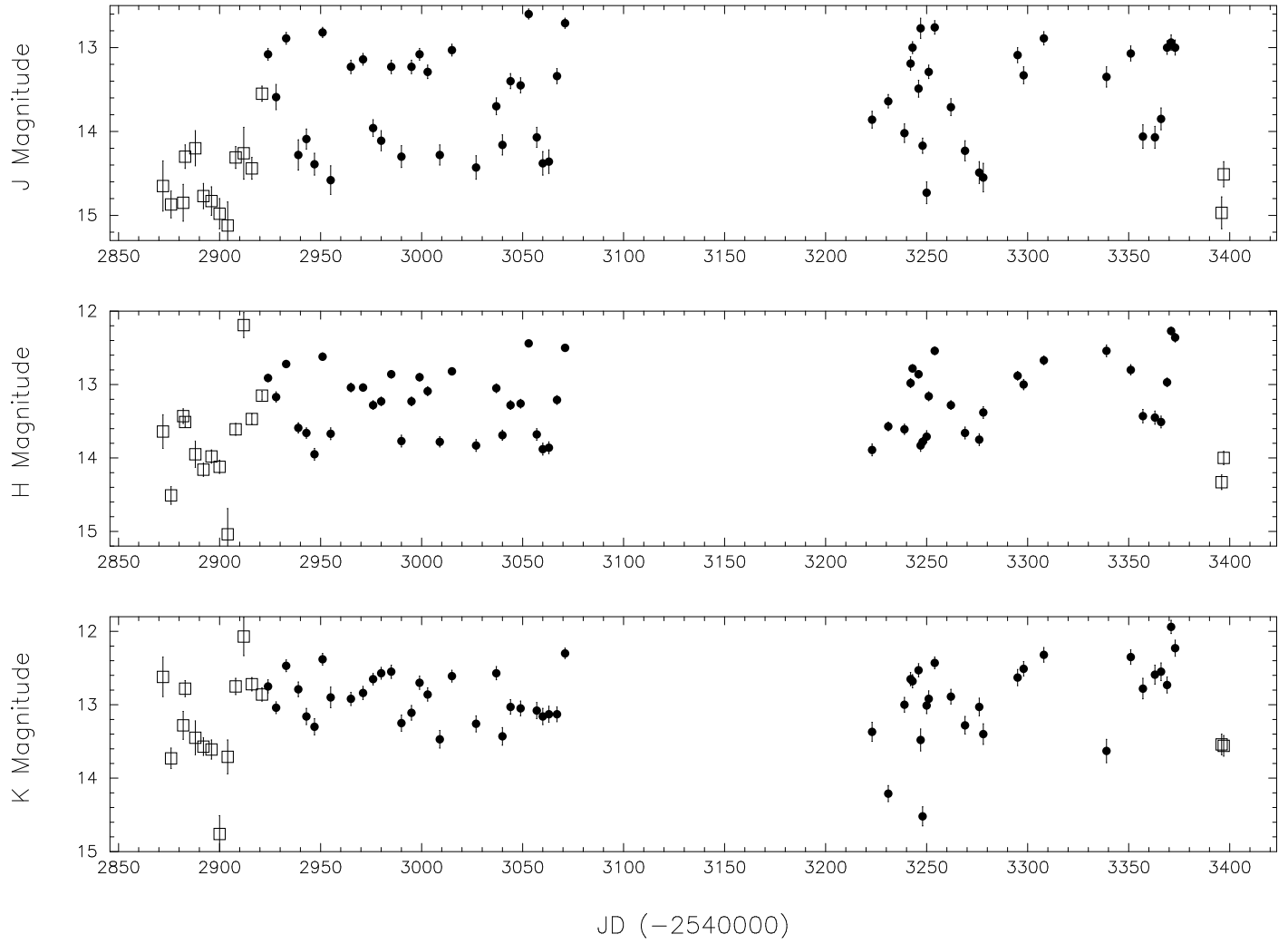


Fig. 2.— Magnitude of BL Hyi in J, H and K Bands vs Julian Date. The state of BL Hyi during each observation, as defined by the optical data, is denoted as follows:  $\square$  Low state;  $\bullet$  High state.

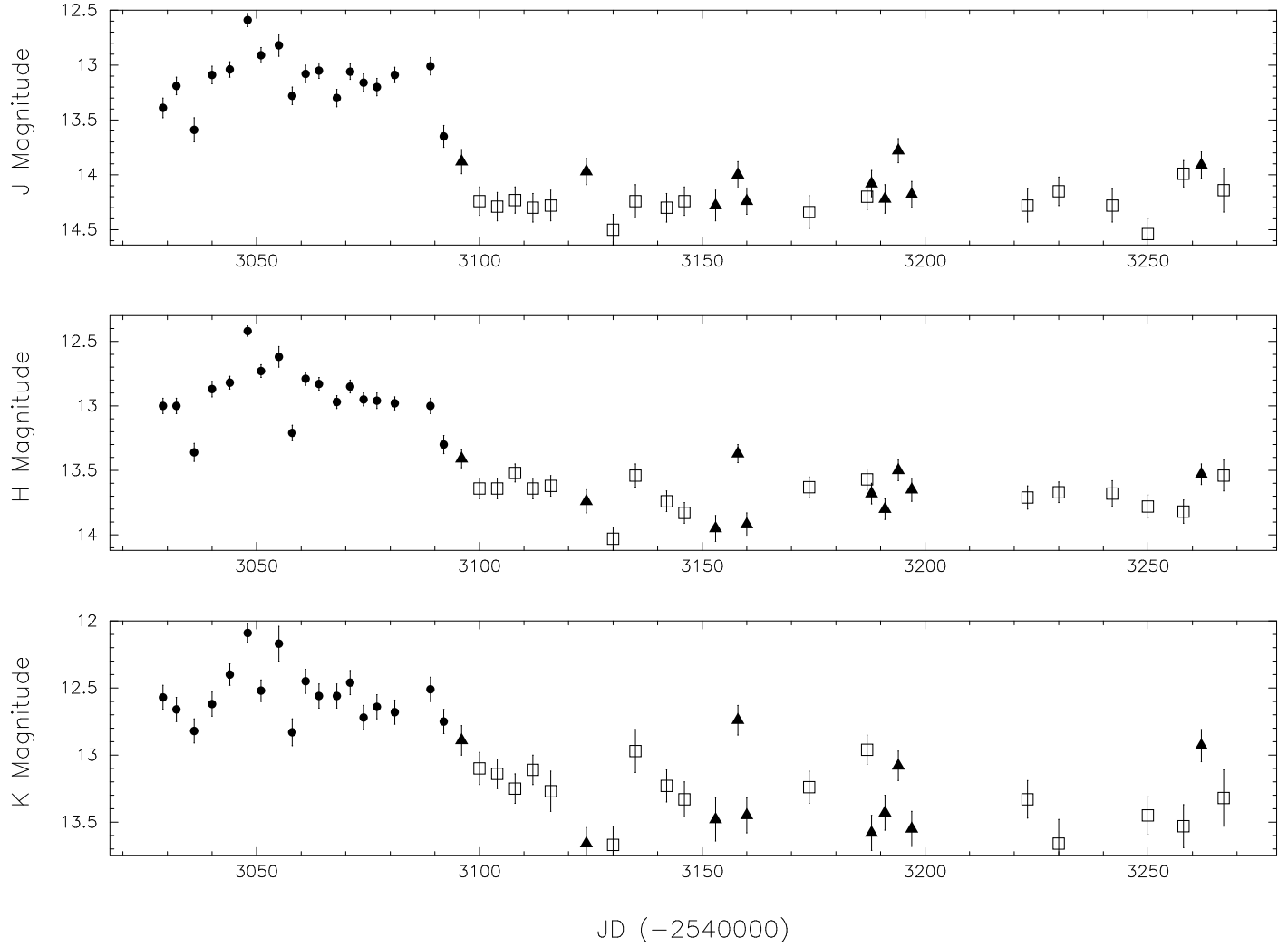


Fig. 3.— Magnitude of V834 Cen in J, H and K bands vs Julian Date. The state of V834 Cen at the time of the observation, as defined by the optical data, is denoted as follows:  $\blacktriangle$  Transition;  $\square$  Low state;  $\bullet$  High state.

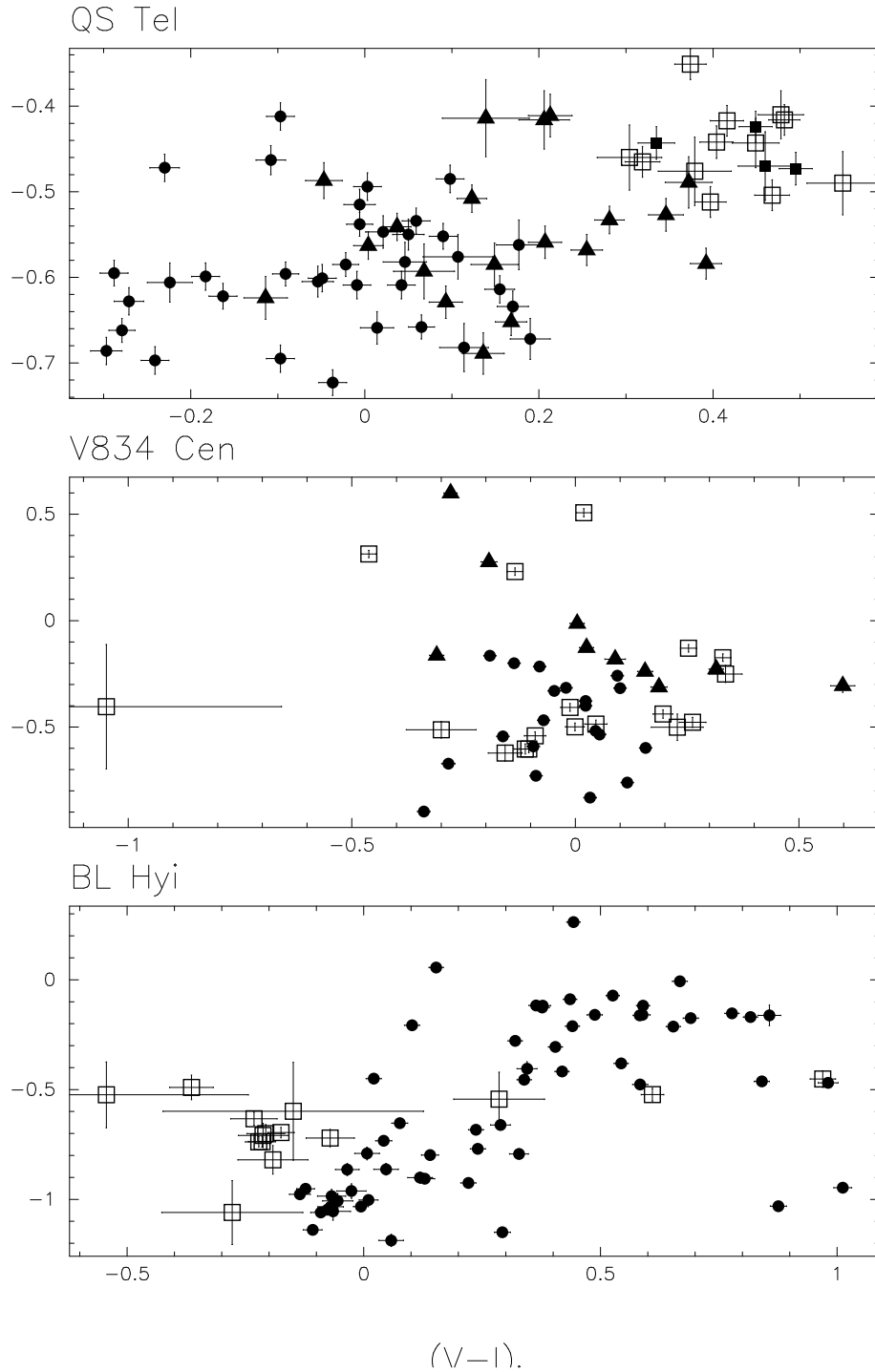


Fig. 4.— Color-color plots in the optical for the three polars. The state of the polar during an observation, as defined by the optical data, is denoted as follows:  $\blacktriangle$  Transition;  $\square$  Low state;  $\bullet$  High state.

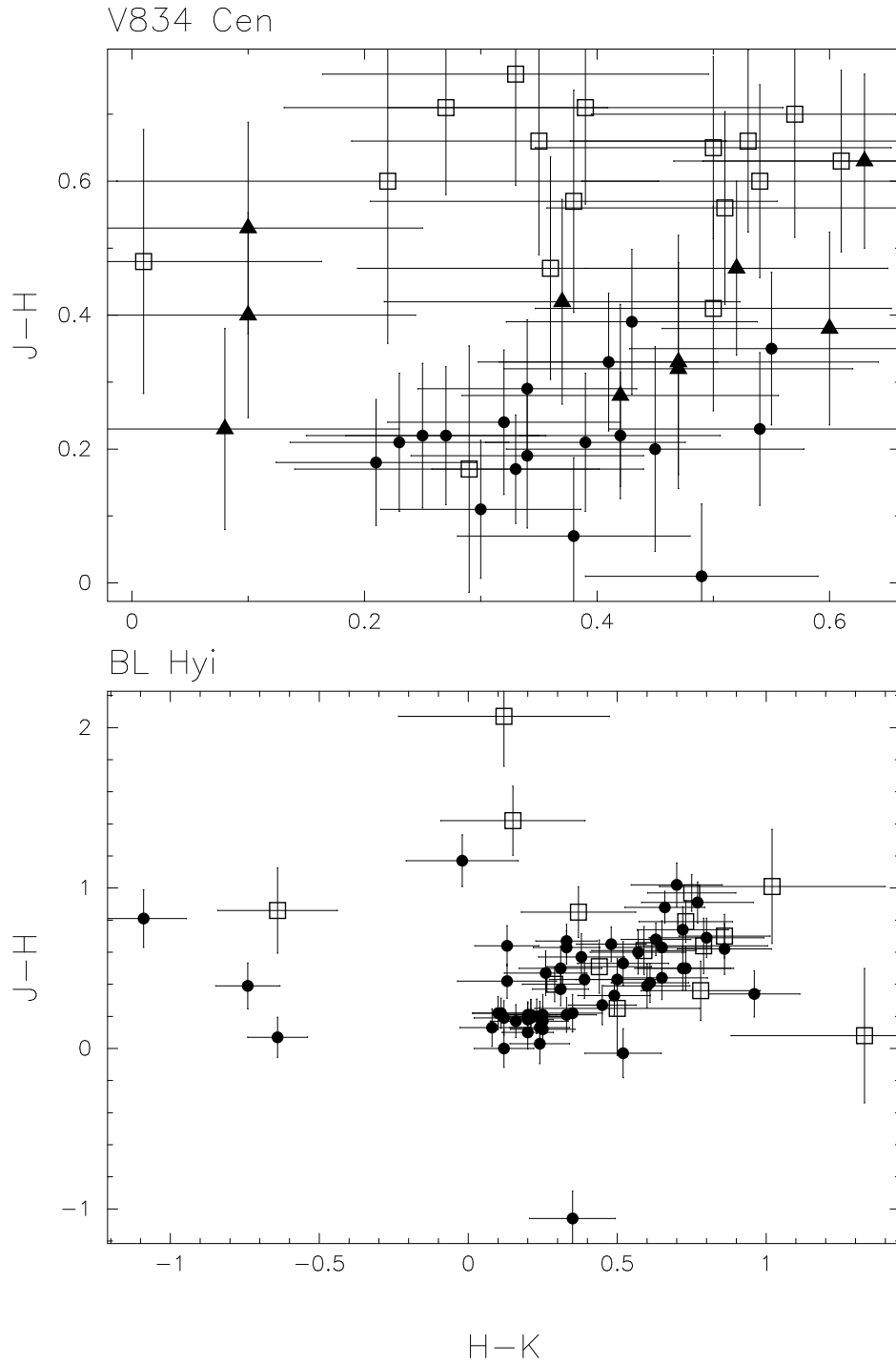


Fig. 5.— Color-color plots in the near-Infrared for V834 Cen and BL Hyi. The state of the polar during the observation, as defined by the optical data, is denoted as follows:  $\blacktriangle$  Transition;  $\square$  Low state;  $\bullet$  High state.

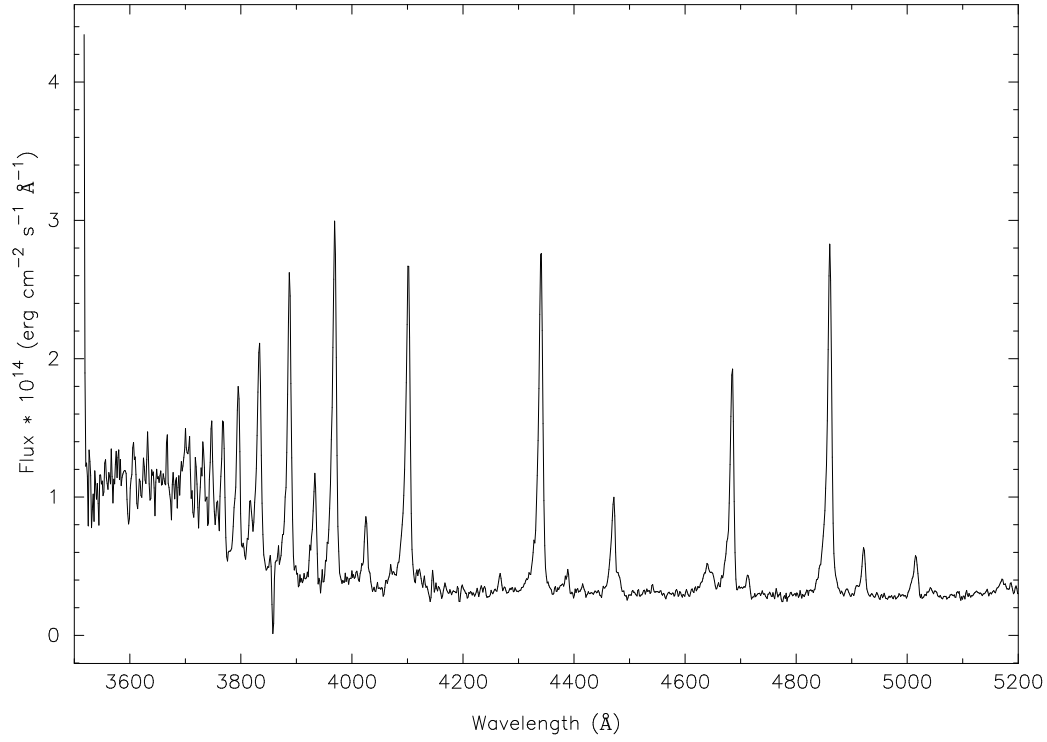


Fig. 6.— High State spectrum from BL Hyi obtained on 2004 Sept 15.

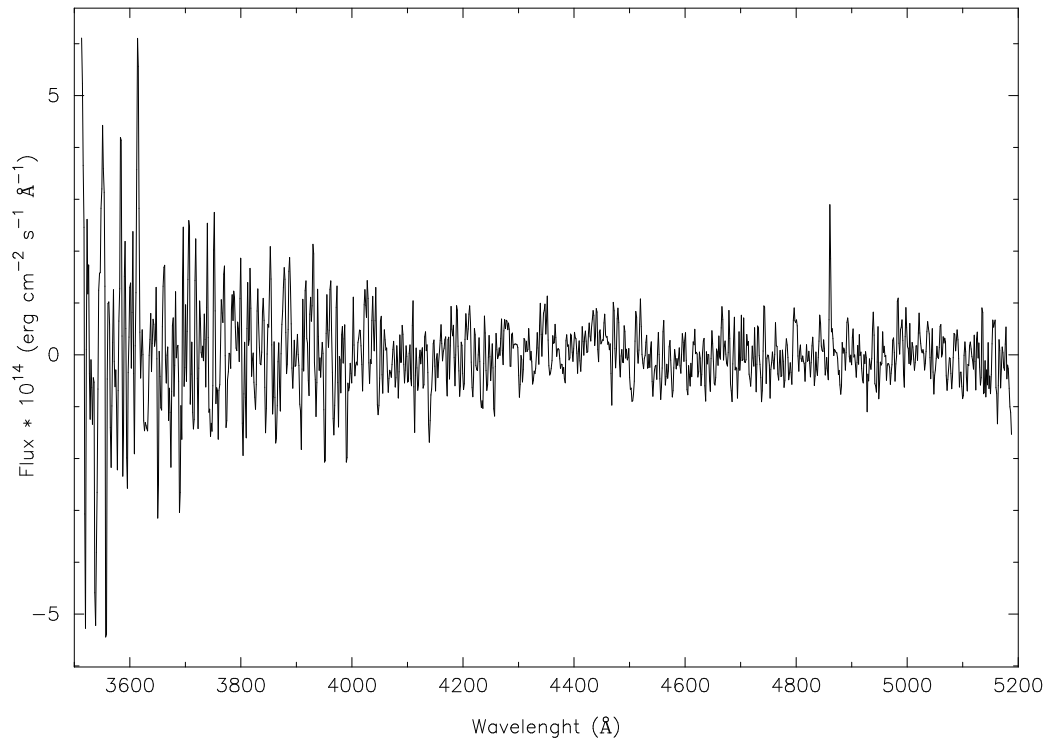


Fig. 7.— A low state spectrum from BL Hyi averaged from seven observations.

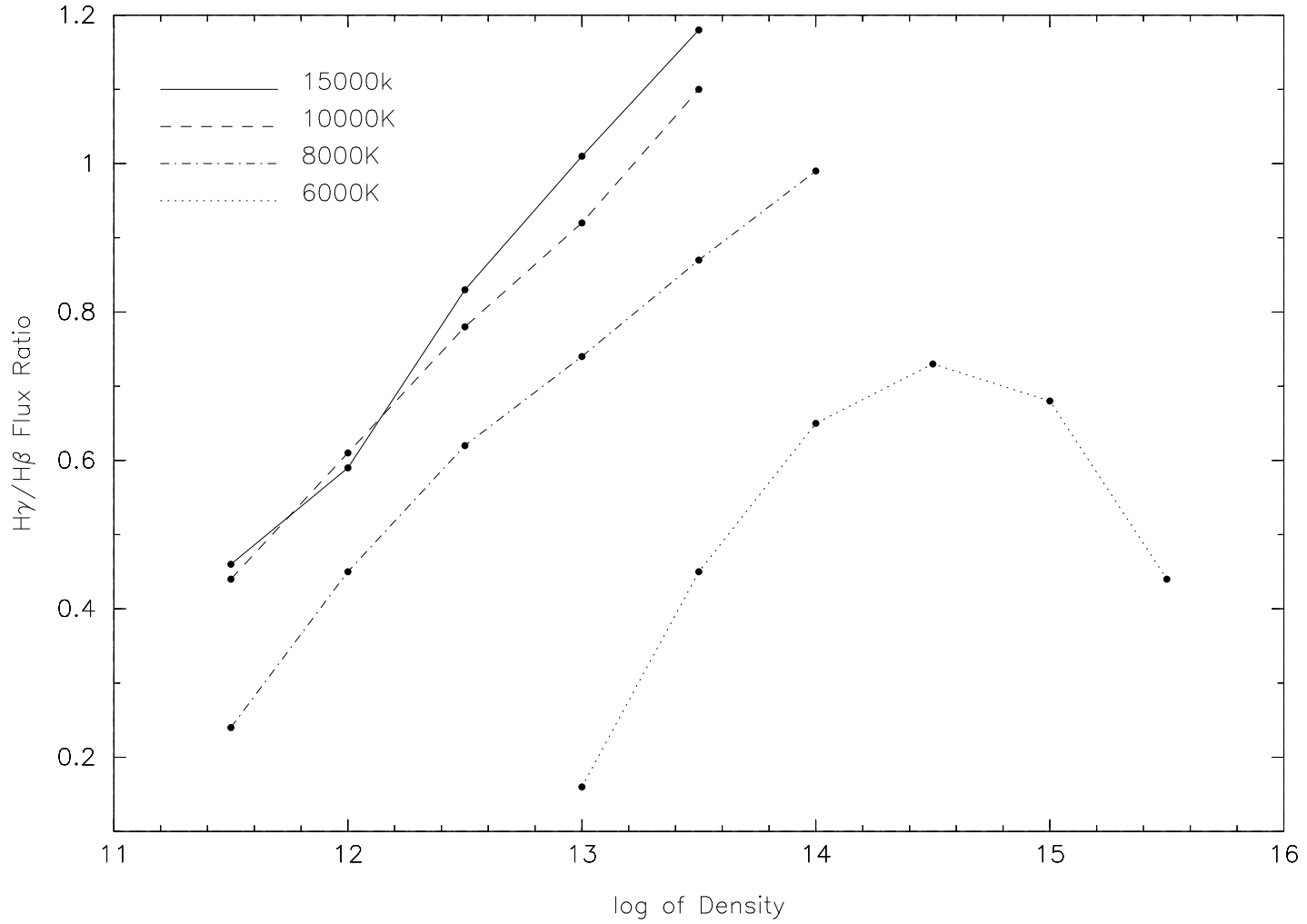


Fig. 8.— Balmer Decrement ( $H\gamma/H\beta$ ) vs Log of Density ( $\text{g}/\text{cm}^3$ ) for various temperatures from Williams (1991).



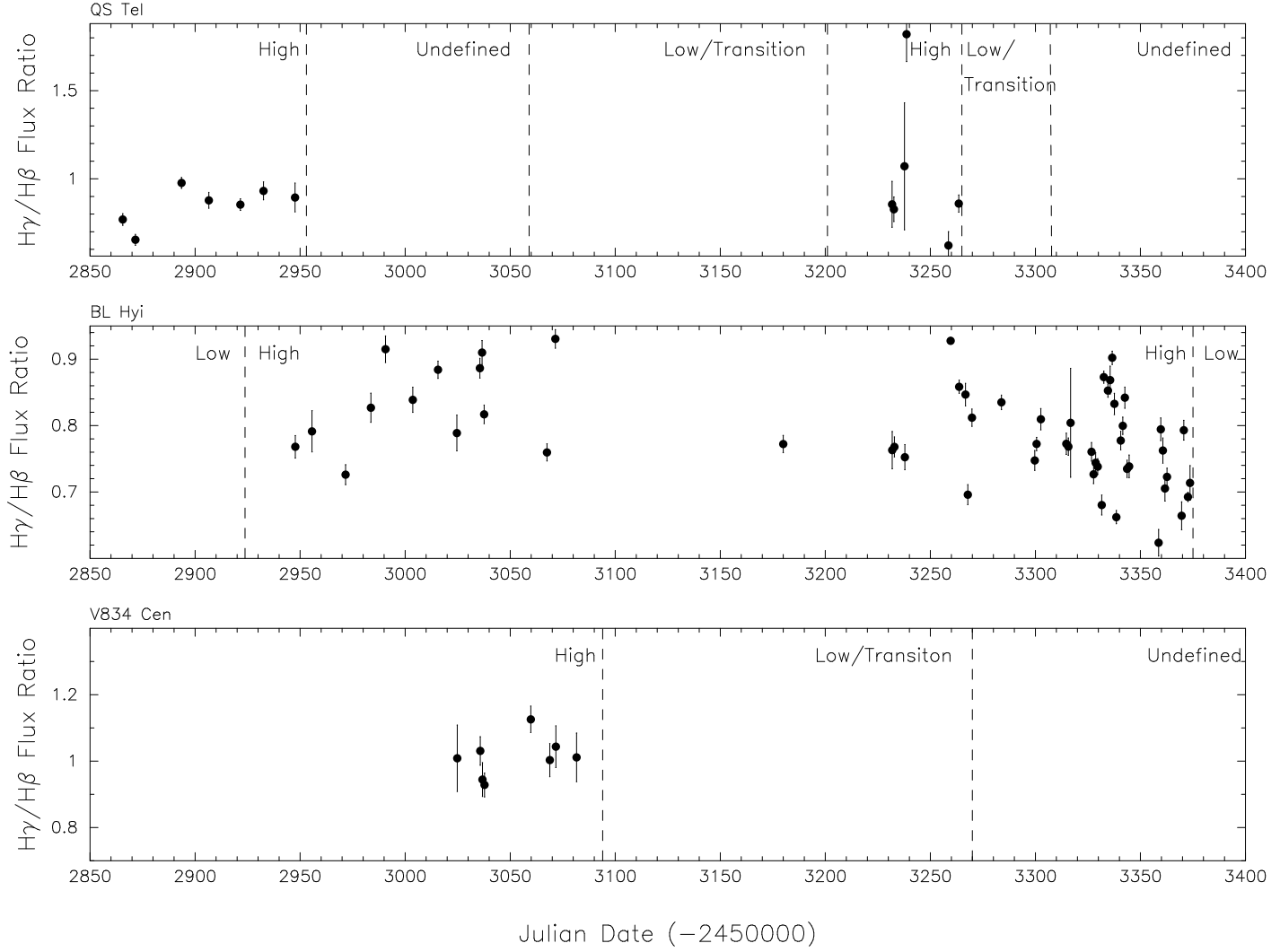


Fig. 9.— Balmer decrement vs Julian date. The state of the polar is marked using the transitions shown in Figure 1. The Balmer decrements are only defined in the high state (see Table 3).

## REFERENCES

- Araujo-Betancor, S. et al. 2005, *ApJ*, 622, 589
- Cropper, M. 1990, *Space Sci. Rev.*, 54, 195
- Ferrario, L., Wickramasinghe, D. T., Bailey, J., Hough, J. H., Tuohy, I. R. 1992, *MNRAS*, 256, 252
- Ferrario, L., Wickramasinghe, D. T., Bailey, J. A., Buckley, D. A. H. 1994, *MNRAS*, 268, 128
- Ferrario, L., Bailey, J., Wickramasinghe, D. 1996, *MNRAS*, 282, 218
- Hamuy et al. 1992, *PASP*, 104, 533
- Hamuy et al. 1994, *PASP*, 106, 566
- Howell, S. B., Cash, J., Mason, K. O., Herzog, A. E. 1999, *ApJ*, 117, 1014
- Howell, S. B., Ciardi, D. R., Sirk, M. M., Schwobe, A. D. 2002, *ApJ*, 123, 420
- Kafka, S., Robertson, J., Honeycutt, R. K., Howell, S. B. 2005, *ApJ*, 129, 2411
- King, A. R., Cannizzo, J. K. 1998, *Apj*, 499, 348
- Mauche, C. W. 2002, *ApJ*, 578, 439
- Moon, D., Eikenberry, S. S., Wasserman, I. M. 2003, *ApJ*, 586, 1280
- Oke, B. *Apj*, 99, 1621
- Ramsay, G. et al. 2004, *MNRAS*, 350, 1373
- Rosen, S. R. et al. 2001, *MNRAS*, 322, 631

Szkody, P., Vennes, S., Sion, E. M., Long, K. S., Howell, S. B. 1997, ApJ, 487, 916

Warner, B. 1995, Cataclysmic Variable Stars (Cambridge Astrophys. Ser. 28; Cambridge: Cambridge Univ. Press), chap 6

Williams, G. A. 1991, ApJ, 101, 1929

Wolff, M. T., Wood, K. S., Imamura, J. N., Middleditch, J., Steiman-Camerone, T. Y. 1999  
ApJ, 526, 435